Multimodal Sensor System for Pressure Ulcer Wound Assessment and Care

Ming-Ching Chang, *Member, IEEE*, Ting Yu, Jiajia Luo, Kun Duan, *Member, IEEE*, Peter Tu, Yang Zhao, Nandini Nagraj, Vrinda Rajiv, Michael Priebe, Elena A. Wood, and Maximillian Stachura

***Abstract*—We present a multimodal sensor system for wound assessment and pressure ulcer care. Multiple imaging modalities including RGB, three- dimensional (3-D) depth, thermal, multispectral, and chemical sensing are integrated into a portable hand-held probe for real-time wound assessment. Analytic and quantitative algorithms for various assessments including tissue composition, wound measurement in 3-D, temperature profiling, spectral, and chemical vapor analysis are developed. After each assessment scan, 3-D models of the wound are generated on the fly for geometric measurement, while multimodal observations are analyzed to estimate healing progress. Collaboration between developers and clinical practitioners was conducted at the Charlie Norwood VA Medical Center for in-field data collection and experimental evaluation. A total of 133 assessment sessions from 23 enrolled subjects were collected, on which the multimodal data were analyzed and validated with respect to clinical notes associated with each subject. The system can be operated by nontechnical caregivers on a regular basis to aid wound assessment and care. A web portal front-end was developed for clinical decision and telehealth support, where all historical patient data including wound measurements and analysis can be organized online.**

***Index Terms*—Chemical vapor sensing, multimodal sensor system, multispectral, pressure ulcer, RGB+D, telehealth, thermal, wound assessment.**

Manuscript received March 30, 2017; revised September 10, 2017; accepted November 7, 2017. Date of publication December 11, 2017; date of current version March 1, 2018. This work was supported by the U.S. Department of Veterans Affairs Innovation Initiative (VAi2) #302—Multimodality Portable Systems for Pressure Ulcer Prevention and Care. Paper no. TII-17-0600. *(Corresponding author: Ming-Ching Chang.)*

M.-C. Chang was with GE Global Research Center. He is now with University at Albany—SUNY, Albany, NY 12203 USA (e-mail: mchang2@albany.edu).

T. Yu was with GE Research. He is now with Google Cloud (e-mail: yuti@google.com).

J. Luo, P. Tu, Y. Zhao, and V. Rajiv are with GE Global Research Center, Niskayuna, NY 12309 USA (e-mail: jiajia.luo@ge.com; tu@ge.com; yang.zhao@ge.com; vrinda.rajiv@ge.com).

K. Duan was with GE Global Research. He is now with Snap Research (e-mail: kun.duan@snapchat.com).

N. Nagraj was with GE Global Research. He is now with Siemens Healthineers, Erlangen 91052, Germany (e-mail: nandini1224@gmail.com).

M. Priebe, E. Wood, and M. Stachura are with the Charlie Norwood VA Medical Center and the Medical College of Georgia, Augusta University, Augusta, GA 30904 USA (e-mail: michael.priebe@va.gov; maxs@augusta.edu).

Color versions of one or more of the figures in this paper are available online at http://ieeexplore.ieee.org.

Digital Object Identifier 10.1109/TII.2017.2782213

I. Introduction

MULTIMODAL sensor fusion has gained much attention due to the benefits it provides for various detection and recognition tasks [1], [2]. The integration of multiple sensing modalities not only expands the associated features but also enhances the joint analytic capabilities. Multisensor integration has wide applications in situation assessment, knowledge exploration, remote sensing, and healthcare [3].

For hospitalized and mobility-compromised individuals during a prolonged healing process, *wound assessment* is an important area for treatment decisions, as it can directly impact the management of clinical resources to ensure a cost-effective intervention. Furthermore, the immobility of a patient can contribute to the development of *pressure ulcers*, which can impose significant morbidity and mortality. Pressure ulcers are localized injuries to the skin and underlying tissue usually over a bony prominence, as a result of direct pressure or in combination with shear forces. According to the National Pressure Ulcer Advisory Panel, 2.5 million pressure ulcers are treated annually in the United States in acute care facilities, resulting in US expenditures of $11 billion per year [4]. Even with the best preventive measures, pressure ulcers can occur, and healing is not guaranteed. In practice, such prolonged treatment processes often require frequent, inconvenient, and expensive clinical visits, where the assessments performed by clinicians can be tedious and overwhelming [5]–[7]. Therefore, an effective and preferably *automatic* means of wound assessment is needed for treatment management.

In this work, a noninvasive wound assessment system based on the integration of multimodal sensors to assess healing progress and assist with treatment management was developed. We incorporated a wide spectrum of sensing modalities (see Fig. 1) including (i) electro-optic (EO, or RGB color), (ii) three-dimensional (3-D) depth (or range), (iii) thermal/IR, (iv) multispectral, and (v) chemical vapor sensing into an assessment probe, which combines heterogeneous and comprehensive analytical capabilities for wound assessment. Fig. 1(b) and (c) shows the developed sensing probe and apparatus of this study. Our system provides assessment of the wounds in the following aspects: tissue composition, 3-D modeling of the skin surface for wound size measurement, wound-skin temperature profiling, spectral analysis of biological factors, and wound radio-frequency identification (RFID) vapor analysis. Automatic algorithms are developed to jointly analyze the multimodal

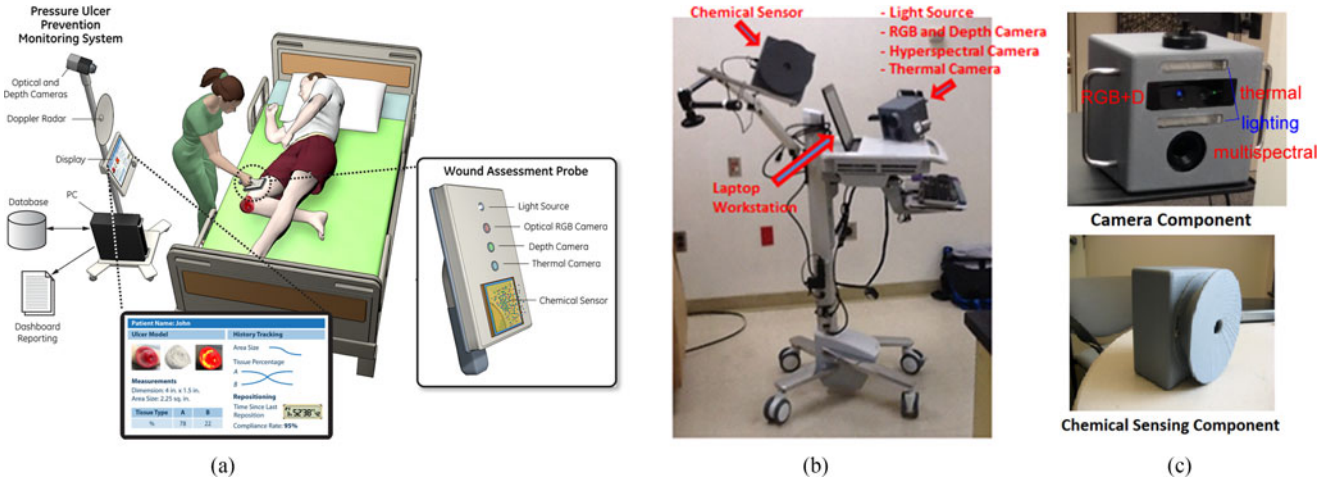

Fig. 1. Overview of the multimodality portable system with the integration of optical, range, thermal, multispectral, and chemical sensing for pressure ulcer *wound assessment* and care. (a) shows a schematic plot. (b) is the developed hand-held probe with the computer system. (c) shows the multimodal camera probe and the chemical sensing component.

measurements. Our measurements correlate strongly with the wound healing trends, thus they can serve as a predictive indicator.

Main contributions of this paper are fivefold.

1) Our multimodal system is by far the first of its kind with respect to multisensor fusion for the integration of five sensing modalities for joint assessment. In comparison, existing assessment systems typically make use of one [6]–[8], two (RGB+D [9] or RGB+laser [10] sensor fusion), or at most three modalities [11], where the cross-modal investigation on sensor fusion is limited.
2) We have applied multispectral sensing to human biological oxygenation analysis. Previously this approach has mostly been applied to physical domains such as remote sensing. Similarly, we have demonstrated that chemical vapor sensing can be applied to human odor analysis. Previously the technology has only been applied to material fragrance analysis (but not human subjects). We believe this is the first attempt of applying these modalities on live human subjects in a clinical setting.
3) We developed an interactive system for the quantitative measurements of wounds in multiple clinical aspects including surface, depth, volume, tissue composition, thermal profiling, spectral analysis, and chemical RFID vapor analysis, all with minimal user intervention. We further investigated the correlation between the multimodal assessments and the healing trends. To the best of our knowledge, this is the first demonstration in a clinical setting.
4) Evaluations are performed on a clinical dataset at an in-field clinical pressure ulcer treatment site with 108 multimodal scanning sessions from 23 subjects. The larger dataset is not only advantageous in clinical analysis but also necessary to quantify the differences across various scanning modalities.
5) We developed a graphical user interface (GUI) and web front-end to store and organize all historical patient data including wound measurements and assessments, so that clinical decisions and telehealth applications can be well supported.

II. Related Works

Wound assessment tasks typically include the analysis of: (1) *geometric* parameters of the wound i.e., length, width, depth, area, and volume, (2) *physiological* aspects of the wound i.e., pressure, degree of wound perfusion and percentage of tissue types, and (3) *biochemical* peculiarities i.e., concentration of enzymes involved in tissue degradation [12]–[15]. In current practice, wound assessment still relies on visual inspection and manual measurement by clinicians. Wound dimensions (length and width) are measured by rulers, and wound area is approximated with regular shapes such as rectangles or ellipses [11]. Manual reading of wound measurements can be inaccurate and inconsistent. Intrusive wound volume measurement methods including moulds and saline infusion require injection of materials into the wound, which are both uncomfortable and inaccurate due to absorption by wound tissue [11], and can carry high risk of cross contamination and infection [5]. Manual assessment of wound healing progress can be subjective, and clinical expertise can be hard to formalize.

Image processing techniques have been applied to visual wound assessment for (1) automatic quantification of wound shape and measurements [8], [10], [16], and (2) skin tissue classification [6] to estimate wound severity or burn degree [5], [7], [17]. See [8] for a detailed survey. Recent studies have incorporated thermal or IR cameras for wound assessment [11], [18], since skin temperature is an important factor that controls the rate of metabolism of cells and tissue engaged in the wound repair process. Multispectral sensing has great promise in biological analysis based on its capability to 'see through' the skin and characterize factors such as the blood oxygen saturation [19]. In chemical sensing, GC-MS [20] is a versatile vapor sensing technique with wide applications

including pollutant monitoring, fragrance analysis, security, and forensic investigations. On the other hand, passive RFID sensing based on impedance spectrum analysis [21], [22] is useful in biopharmaceutical process monitoring.

Although various sensing modalities (RGB, depth, thermal, multispectral, and chemical sensing) have been applied for wound assessment for individual studies, a comprehensive joint exploration among these modalities is still lacking. In our pilot study, we collected a large multimodal clinical dataset, on which a comprehensive assessment system was developed.

III. Multimodal Wound Assessment and Analysis

We have developed a multimodal probe system for wound assessment that can be operated by nontechnical caregivers on a regular basis. A GUI is developed to simultaneously visualize all scanning views in real-time. This is particularly appealing for prompt visual feedback and a better user experience. Figs. 4–7 depict parts of the GUI for the operations of each respective modality.

The use of multiple sensing modalities is advantageous not only for the combination of a richer sensing array, but also because *heterogeneous strength can be leveraged in a bootstrapping manner which jointly enhances overall sensing capabilities*. To illustrate, RGB optics is useful for wound localization, segmentation, and tissue classification; depth sensing is suitable for 3-D shape modeling; thermal can be used for blood flow and metabolic activities; spectral analysis can better reflect biochemical factors such as oxygen saturation; and chemical sensing can measure skin odor intensities.

To effectively make use of multimodal sensing, *cross-modal registration* is required. Camera registration is performed as a one-time effort during system assembly, to obtain cross-sensor calibration parameters. The registration step enables the alignment and rectification of sensing views into a common coordinate system. For example, RGB views can be aligned with depth maps to create a 3-D reconstruction with texture mapping, and thermal maps can be overlaid on top of the 3-D wound model for further analysis. Without proper registration which leads toward fusion of heterogeneous sensing modules, the system with simple combination of sensors will not work well.[1]

Registration between RGB and depth comes with the Creative Intel Senz3D camera during its manufacturing process. This registration can be done similarly to our approach in registering RGB and thermal cameras, by using standard landmark matching and warping [23] methods. To calibrate between thermal imaging and RGB/Depth camera views, we leverage a flat metal surface with small holes. Since thermal imaging reflects the temperature surface significantly between the metal surface and empty holes, it becomes trivial to identify the landmark correspondences between the thermal images and RGB/Depth camera views, thus solving the thermal imaging camera calibration problem.

[1]We note that cross-modal registration provides crucial information for sensor fusion, which enables us to bootstrap multi-sensor capabilities in our system. To clarify, there are tasks that can be performed well without sensor fusion. For example, after tissue segmentation, the classification of wound tissues can be done reasonably well solely in the RGB view. Chemical sensing is performed separately from all other modalities.

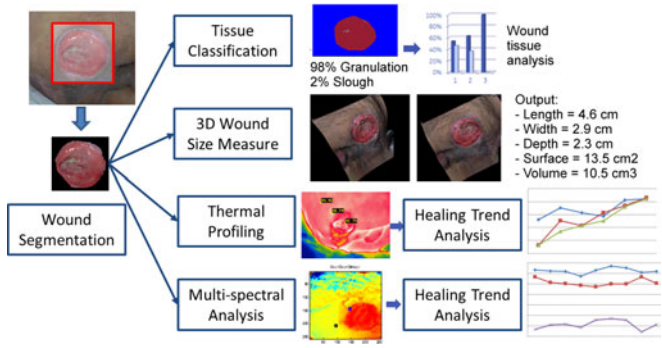

Fig. 2. Multimodal wound assessment workflow.

Our multimodal assessment pipeline consists of the following steps, which are also summarized in Fig. 2.

A. Wound Segmentation and Tissue Classification

consist of three steps: (i) The region of interest (ROI) is manually selected as a bounding box of the wound(s) of interest from the RGB view. (ii) The selected ROI then triggers the wound segmentation algorithm to automatically delineate a refined wound mask. This segmentation step can be repeated and is further refined until a satisfactory wound mask is obtained. (iii) Tissue classification is performed within the wound region, where tissue labels including granulation, slough, eschar, and bone/tendon are calculated. (Section III-F)

B. 3-D Modeling for Wound Measurements

The above wound segmentation mask is projected to the depth view to delineate a 3-D point cloud, which is used to reconstruct a 3-D model of the wound. Wound size measurements including length, width, depth, and surface area can be directly calculated. (Section III-G)

C. Thermal Analysis

The wound segmentation mask is then projected to the thermal view to identify the wound bed (note that wound segmentation is not feasible on the thermal modality alone). Thermal analysis is performed to compare the temperature differences between the wound bed, wound periphery, and normal skin. We will show that this *peri-wound* thermal analysis leads to strong correlation with the healing trend. (Section III-H)

D. Multispectral Sensing

captures the reflectance spectra of the skin that can effectively characterize biological factors including hemoglobin *oxygen saturation* (SO2) of the wound, which is correlated with the healing process. Our spectral analysis is again performed with the guidance of the wound segmentation mask to calculate the SO2 for both the wound bed and normal skin for healing status estimation. (Section III-I)

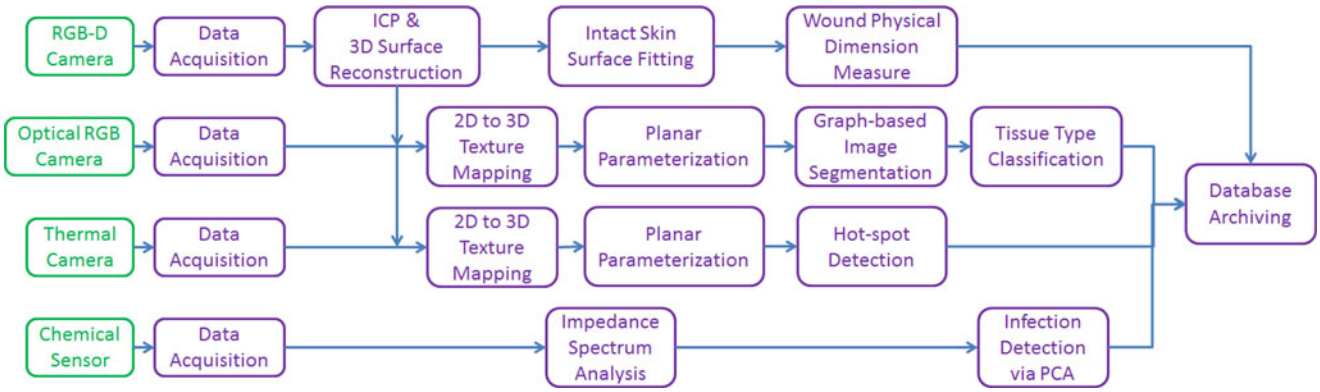

Fig. 3. Data workflow diagram showing the detailed workflow for the multimodal sensor data processing, fusion, and decision making steps. The algorithms and parameters of these steps are explained in each of the subsections in Section III.

E. Chemical Sensing

measures the RF signals in response to wound vapor. By comparing the difference between the assessments among open air (as a baseline) and wound odor intensities, we establish correlations with the healing status. Measurements across sessions in time also reveals the overall healing trend. (Section III-J)

Each of our sensing modalities produces an estimate of the wound regarding the healing trend either independently or jointly. 3-D wound modeling yields accurate measurements that directly correlate with the healing status. Our thermal, spectral, and chemical analyses each yields an estimate of the healing trend.

Fig. 3 depicts a detailed workflow for the multimodal sensor data processing, fusion, and decision making steps. The following subsections provide details regarding each of the assessment processes, including the algorithms and parameters used in each of the sensing modalities.

F. Wound Segmentation and Tissue Classification (RGB)

We developed an interactive *wound segmentation* method with minimal user interaction using *GrabCut* [24] to effectively segment wound pixels from the normal skin pixels in the RGB view. The operator provides three steps of inputs during the interaction process:

1) a bounding box surrounding the wound [see blue box in Fig. 4(a)],
2) a polyline defining the wound region [see red curve in Fig. 4(a)] and
3) another polyline for the normal skin in the background [see green curves in Fig. 4(a)].

Our system then constructs an initial wound (foreground) and peripheral skin (background) model using mean shift methods [25]. A graph partitioning algorithm then automatically calculates a wound segmentation mask as in Fig. 4(b). This procedure can be repeated for a number of iterations until a satisfactory segmentation is obtained.

Afterwards, *tissue classification* is performed using a three-step approach:

1) a mean shift segmentation is performed on the wound tissue pixels to obtain a set of fine-grained regions,
2) for each region, color histogram features are extracted for use in tissue classification,
3) each region is labeled with one of the four predefined types — *granulation*, *slough*, *eschar*, or *bone/tendon*, using a random forest classifier. Fig. 4(c) shows an example of a result depicting calculated tissue percentages of the wound.

G. 3-D Wound Size Measurement (RGB+D)

We use a lightweight off-the-shelf RGB+D camera, the Creative Intel Senz3D RGB+D camera[2] for its small form factor and portability. This camera performs depth sensing using "time-of-flight" technology, in that it measures the infrared light pattern travel time and thus distance between camera sensor and the sensing object surface.

From the RGB wound segmentation and the registered depth view, we construct a 3-D model of the wound with texture mapping, where wound size can be directly measured [see Fig. 5(a)]. Note that the raw signal from the depth view is typically noisy and can contain many holes and artifacts. To this end, the wound regions from the depth view are initially represented as a 3-D point cloud. However, volumetric measurements, and texture mapping requires a surface mesh (i.e., two-manifold). Surface reconstruction from an arbitrary point cloud is known to be an ill-posed problem [26]. Popular methods including the *ball pivot algorithm* [27] are typically erroneous with respect to irregularities and outliers. The Poisson surface reconstruction methods [28], [29] produce a water-tight surface mesh where the optimization is cast as a spatial Poisson problem. Although the Poisson surface mesh is plausible for visualization and texture mapping, its enforcement of the "water-tightness" can cause artifacts due to extrapolation of missing data. In our case, the wound surface can be reconstructed as in Fig. 5(b), however the Poisson surface is still not sufficient for the volumetric measurement of the wound. To this end, we approximate the exact 3-D wound surface using the *convex hull* of the 3-D wound point

[2]https://us.creative.com/p/web-cameras/creative-senz3d

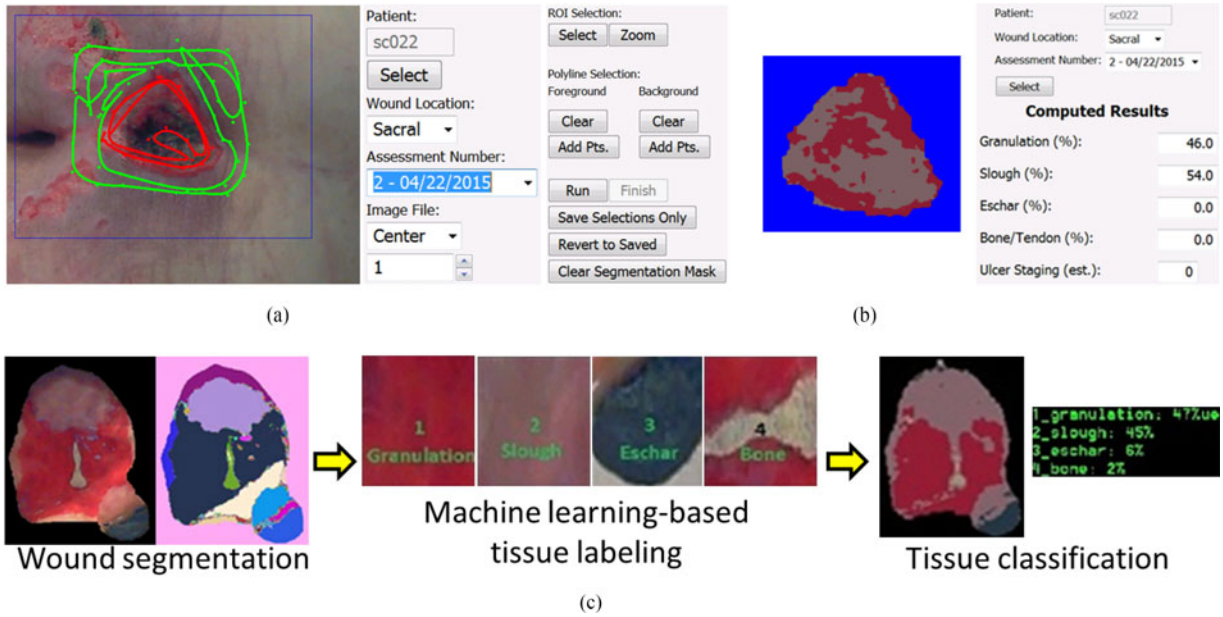

Fig. 4. Wound segmentation and tissue classification are performed (a) by semiautomatic segmentation using *GrabCut* via the GUI followed by (b) automatic tissue classification. (c) Workflow.

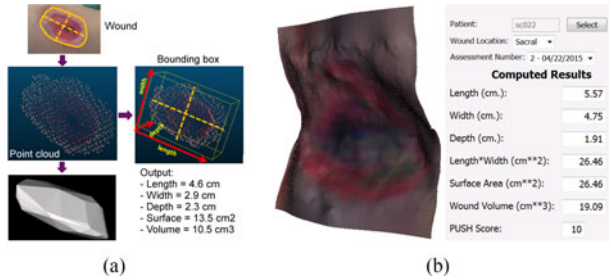

Fig. 5. 3-D reconstruction of the wound surface for size measurement. (a) shows the workflow. (b) shows the reconstructed 3-D wound surface for quantitative measurements.

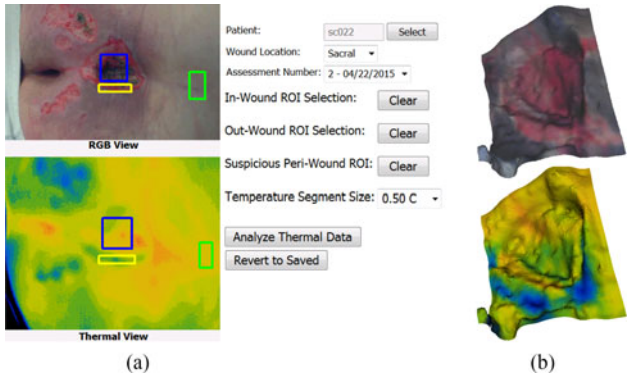

Fig. 6. (a) Peri-wound thermal analysis via manual ROI selection using the GUI. Green ROI box depicts a normal skin baseline region, blue depicts the ROI inside the wound bed, yellow depicts the ROI at the wound periphery, where thermal measures are calculated. (b) 3-D surface meshes with (upper) RGB and (bottom) thermal rainbow texture maps.

cloud similar to [16]. The computation of the convex hull from 3-D points is not only fast [30] but also sufficiently accurate for volume estimation. Fig. 5(a) depicts the workflow, and Fig. 5(b) shows the 3-D wound model along with quantitative measurement results shown in the GUI. Users can manually rotate the surface mesh and measure distances between any two points in the view. In Section IV-A, we will compare our automatic wound size measurement with manual measurements from the clinicians and analyze such measurements using Pearson correlation analysis.

H. Thermal Analysis

Infrared thermography provides a means to inspect a wound beyond the visual spectrum. Motivated by the knowledge that wound repair mostly occurs at the periphery, where biochemical metabolism for tissue repair is most active, the observed temperature at the wound periphery (or *peri-wound* in short) should be higher than at normal skin. We thus focus on measuring the *relative* temperature differences between the wound bed, peri-wound, and normal skin to derive measures used for healing trend estimation. We use the Micro Epsilon ThermoIMAGER TIM 400 infrared camera with 38° optics as our thermal/IR sensor.

Our interactive thermal analysis workflow relies on manual specification of three ROI boxes: (i) the wound bed, (ii) the peri-wound, and (iii) the normal skin, as shown in Fig. 6(a). The cross-modality registration and calibration is again useful here for several reasons: (1) The ROI selections can be performed on the RGB view and then projected to the thermal view, otherwise direct ROI delineation on the thermal view is not feasible. (2) Wound segmentation masks obtained from the RGB view can be used to visually guide the peri-wound ROI delineation. (3) A 3-D model of the wound with thermal mapping can be visualized as in Fig. 6(b).

After the above ROI boxes are obtained, average temperatures of the wound bed T_w, peri-wound T_p, and normal skin T_s are calculated. We extract two features $f_p = T_p - T_s$ (the peri-wound temperature difference feature) and $f_w = T_w - T_s$

(the wound temperature difference feature) for healing trend estimation. In the case of a large wound bed, the temperature distribution of the wound bed can vary significantly. We thus add a third feature f_σ as the temperature variance of the wound bed. Note that all three temperature features are invariant across subjects and the scanning conditions. We can thus aggregate all collected observations and perform *logistic regression* as a form of future healing trend analysis. Section IV-C will provide further details with experimental validations.

I. Multispectral Oxygen Saturation (SO2) Analysis

We use the BaySpec Compact OCI-2000 Snapshot Spectral Imager to acquire the spectral image sequence of a wound within a band of near IR wavelengths from 600 to 1000 nm at a high video framerate. In contrast to EO sensing, where only three wavelength bands (RGB) are captured, this multispectral sensor captures 27 spectral bands, which can be viewed as an extension of the three (RGB) bands to a wider span with more bands at higher precision. Multispectral imagery captures the reflectance spectra of the skin, which can effectively characterize a number of biological factors including oxygen saturation of blood, tissue thickness, and the scattering properties of tissue [19]. For the assessment of wound healing status, blood flow increase is part of the initial inflammatory and proliferative stages for general wound repair. Clinical literature suggests that blood flow or oxygen supply should be higher in the wound bed than at the wound periphery [31]. Based on this argument we developed our spectral analysis algorithm for healing assessment.

To analyze the multiband images, we adopt a popular model based on the *Beer–Lambert Law* [32] to estimate the concentration of *oxygenated hemoglobin* h_o and *deoxgenated hemoglobin* h_d of the wound, by calculating the light attenuation spectrum A at each pixel (i, j). According to light diffusion theory, the tissue attenuation spectrum can be expressed as the logarithm of the ratio of incident light intensity I_o to reflected light intensity I_r. Beer's law describes the relationship between the concentration of the absorbers, and the incident and reflected light intensity. The measured attenuation A is generalized to calculate h_o and h_d. The *oxygen saturation* (SO2) at each pixel (i, j) represents the hemoglobin concentration, which is estimated as $\mathrm{SO2}(i, j) = \frac{h_o}{h_o + h_d}$. The SO2 effectively measures the level of oxygen supply at each wound pixel, and thus is strongly correlated with blood flow across the wound and the healing trend.

We found that sufficient illumination during multispectral scanning is crucial to ensure data quality. This is reasonable since spectral sensing produces many bands of images, and the exposure of light captured by each filtered band is limited compared to other sensing modalities. Environmental and lighting conditions can affect the raw multispectral signals, such that the absolute pixel values may not be consistent across scans. To this end, we apply a similar *baseline* strategy as in our thermal analysis. We store an initial baseline map for each subject, which is used to normalize all scanning sessions accordingly. As shown in Fig. 7(a), we provide a GUI for the user to select (i) the wound ROI, (ii) the normal skin ROI, and (iii) an option to specify the baseline normal skin ROI or load from existing scans. The system will automatically normalize all measurements with respect to the baseline to calculate the spectral maps for subsequent analysis, including the calculation of SO2.

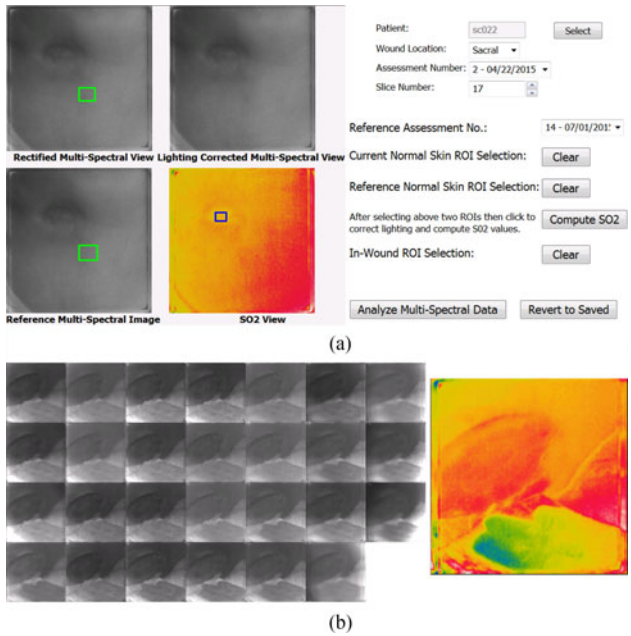

Fig. 7. Multispectral oxygen saturation (SO2) analysis. (a) GUI for multispectral baseline selection and analysis. (b) The 27 spectral bands after baseline normalization and the computed SO2 map based on the Beer–Lambert model, where red depicts higher SO2 values.

J. Chemical Vapor Sensing Analysis

Skin wounds and pressure ulcers are known to have distinctive odors. This is based on anecdotal evidence and feedback from nurses and health care providers. Based on this evidence, we have developed a chemical sensing module equipped with a vapor sensing unit to analyze odor patterns released from ulcer wounds as a feature for wound assessment. Data collection and experiments are performed under IRB approval.

We incorporated two noncontact chemical vapor analysis modules. (i) A *Radio Frequency (RF)* based chemical sensor was designed for in-line assessment use. The RF chemical sensor responds to vapors released from the ulcers based on changes in the dielectric properties of the sensing film, which essentially measures the changes in the impedance and frequency response of the resonant RF spectrum. (ii) We further included a vapor absorption pad with medically approved gauze for the collection of ulcer vapor data in order to perform off-line *Gas Chromatography/Mass Spectrometry* (GC-MS) [20], [33] measurement analysis.

For chemical sensing, Fig. 9(a) and (b) shows the chemical instruments that were used in this study. Both (1) a bench-top GCxGC MS instrument—The LECO Pegasus 4-D GCxGC TOFMS with in-house sample preconentrator and Gerstel TDSA, and (2) a portable instrument— The HAPSITE Inficon GC/MS Chemical Identification System were used. The HAPSITE system is a field-portable instrument with a built-in sample preconcentrator. It contains an additional headspace sampling system. This portable system produces results com-

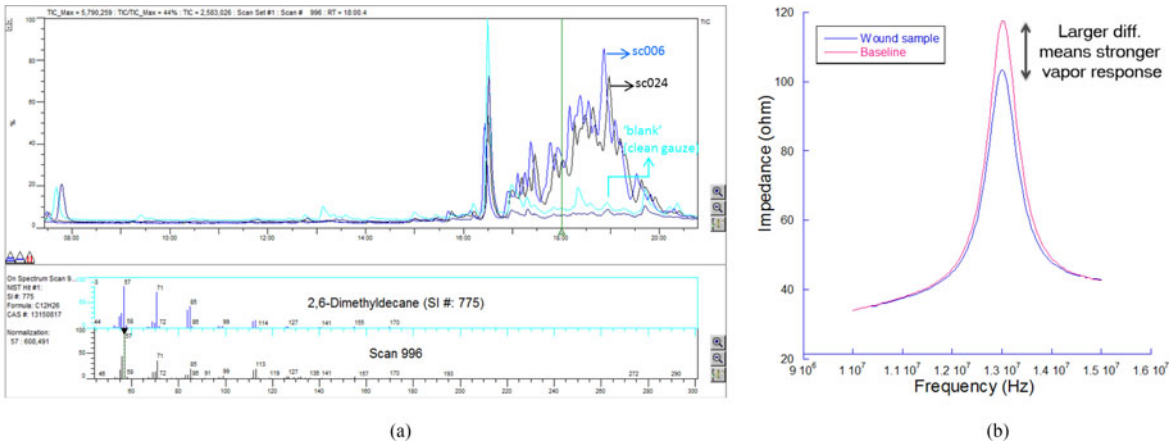

Fig. 8. (a) GC-MS trace for samples from subjects sc006, sc024 compared to a blank sample. (b) Sample RF chemical sensing response pattern.

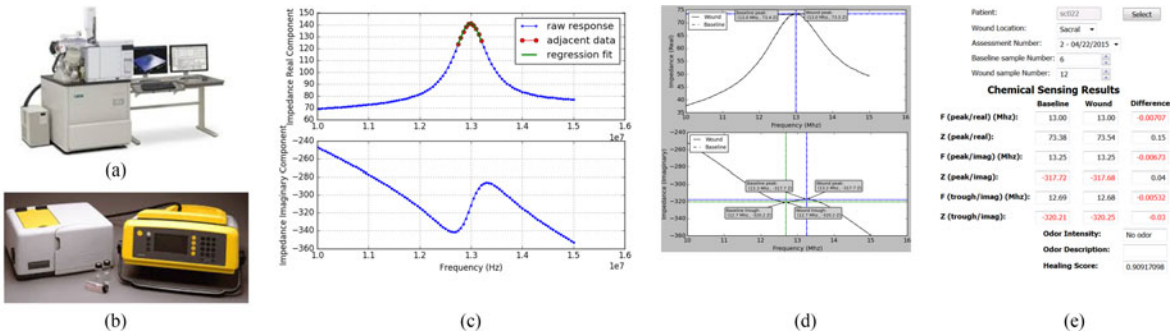

Fig. 9. RF chemical sensing. (a) LECO Pegasus 4-D GCxGC TOFMS bench-top instrument with in-house sample preconentrator and Gerstel TDSA. (b) Portable HAPSITE Inficon GC/MS Chemical Identification System with Head Sampling System. (c) Example RF chemical sensing curve of (left) real and (right) imaginary components. (d) Real-case RF chemical response curve shown in the GUI of our system. (e) GUI designed to analyze the measurements.

parable to the LECO bench-top system. We thus integrated the HAPSITE module into our portable system and used the LECO system for off-like analyses.

In our approach, the RF sensor can capture in-line spectral pattern response from wound vapors. The identity and concentrations of these vapors can be analyzed off-line using the GC-MS method, which also provides a level of ground truth to the in-line RF analysis. As shown in Fig. 8(a) (top), clear differences in the overall chromatogram were observed between a blank and wound "soaked" gauze pads from subjects SC006 and SC024. Fig. 8(a) (bottom) shows an example of one of the vapors identified to be 2, 6-dimethyldecance. Other vapors included both pure and substituted—octanol, dodecanol, undecane, and dodecane derivatives. While preliminary, these results provide insights with respect to chemical and multisensor analysis.

Fig. 8(b) shows a typical complex impedance response from the RF sensor. Significant difference between the baseline (open air) curve and the wound sample curve indicates the response of the vapor released from the wound compared to the former. We perform a standard impedance spectrum analysis in RFID sensing [21], [22], [34] for the extraction of the following parameters from the response curves: (i) peak amplitude and impedance differences between the baseline and wound sample along the y-axis, and (ii) peak frequency difference between the baseline and wound sample along the x-axis. Specifically, six features are extracted for wound healing estimation: namely, the peak shifts corresponding to both the frequency and the impedance of the real peak, as well as the peak shifts corresponding to the imaginary resonant and antiresonant peaks—i.e., *Real-Peak-Shift*, *Imag-Peak-Shift*, *Imag-Through-Shift*, and their corresponding *Impedances*. Fig. 9(d) and (e) shows the GUI visualizing the RF response plots and the calculated parameters.

IV. Case Study Results

Collaboration with clinical practitioners at an in-field pressure ulcer treatment site—The Charlie Norwood VA Medical Center (CNVAMC) and the Medical College of Georgia at Augusta University (MCG/AU) was supported by the US Department of Veterans Affairs (VA). In-field data collection and evaluation was performed at the Spinal Cord Injury Unit (SCIU) at the CNVAMC. Both the practitioners' expertise and inputs as well as access to the clinical notes regarding the subjects in our experiments were valuable in the development of this system. A total of 133 scanning sessions from 23 enrolled subjects were collected in compliance with IRB regulations. We received full consent from all participants in the study. Participants in the study are themselves potential sufferers of future pressure ulcers and would thus be beneficiaries of technologies developed under this program. Captured data was analyzed and validated against clinical notes taken for each subject. In the following

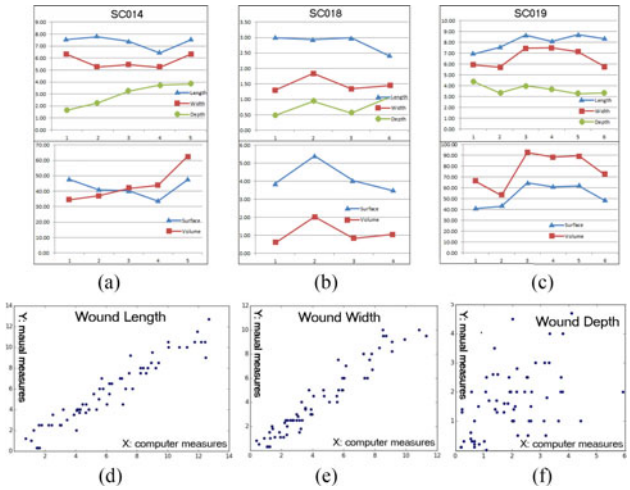

Fig. 10. Example results of (a) wound segmentation, (b) tissue classification, and (c) 3-D model of the reconstructed wound surface with texture mapping.

sections, we select representative cases to discuss in detail to characterize the capability of each sensing modality in terms of wound assessment and healing trend analysis. Key observations regarding these characteristics are discussed.

A. 3-D Wound Size Measurement Results

Our system performs well on wound segmentation and tissue classification; see Fig. 11(a) and (b) for a variety of examples. By keeping track of historical tissue composition of a patient over time, the healing trend can be qualitatively observed. Fig. 11(c) shows examples of 3-D reconstructed wound surface models, where quantitative measurements in terms of wound length, width, depth, surface, and volume can be directly obtained. Fig. 10(a)–(c) shows the historical plots of wound measurements from subjects SC014 (increased size, nonhealing), SC018 (stalled size, nonhealing), and SC019 (increased size, nonhealing) over time. Typically such wound size plots should correlate with the healing trend, however it is not always so—a wound with slightly reduced size can be nonhealing for a prolonged period of time.

We performed *Pearson linear correlation* analysis in Fig. 10(d)–(f) to compare our multimodal algorithmic measurement of wound sizes (length, width, depth) against clinical notes (groundtruth). For the wound length and width, a correlation score of 0.96 was obtained with very small p-values (4.78e-36 and 5.4e-37 respectively). For wound depth, the correlation score reduced to 0.46 with p-value increasing to 1.2e-4. Observe in Fig. 10(d) and (e) that both the wound length and width are strongly aligned with clinical measurements. In comparison, the depth measures in Fig. 10(f) scatter wider and exhibit lower correlation. The variations between the algorithmic and clinical measurements can be attributed to two causes. First manual ruler-based measurement is subjective and tends to be inconsistent. Second manual depth measurement is mostly infeasible and challenging, since it is difficult to measure without physically touching the wound bed. Our clinical partners also confirmed that in general manual wound depth measure is very difficult and inconsistent, which is a well-known issue in current clinical practice. Alternatively, our automatic wound measurement is objective and reliable, as empirically supported by the small p-values.

B. Thermal and Multispectral Healing Analysis Results

We found that peri-wound temperature difference features f_p correlate most strongly with the healing trend. Observe in Fig. 12(a) that the horizontal line of $-2\,^{\circ}$C represents a good, close-to-ideal separation between the healing (blue) and nonhealing (red) cases. We thus propose an empirical rule for healing trend prediction using a threshold of $-2\,^{\circ}$C regarding f_p. In other words, if the peri-wound temperature is more than $2\,^{\circ}$C lower than the normal skin, i.e., $f_p = T_p - T_s < -2$, the wound tends to be nonhealing. We highlight two such nonhealing cases SC005 and SC015 in Fig. 12(a). Additional rules can be added to the list. For instance, large temperature variation in wound bed, i.e., $f_\sigma > 2.5\,^{\circ}$C, also indicates nonhealing.

We performed *logistic regression* based on the three temperature features f_p, f_w, f_σ to perform healing trend estimation and validation. A logistic regressor is trained on labeled data using cross validation. As a result, each feature is associated with regression coefficients indicating the importance of this feature—higher coefficients indicate stronger impact of the feature to the final estimation. The obtained regression coefficient is 1.8798 for f_p, 0.0876 for f_w, and 0.398 for f_σ, respectively. The coefficient for the peri-wound feature f_p is significantly higher, which coincides with our empirical observations. Fig. 12(b) presents the thermal regression results, where an error rate of 23.75% is obtained.

For multispectral analysis, we use the median SO2 value of the wound bed to correlate with the healing status. Biological findings suggest that persistent inflammation at the wound bed impairs the healing process, thus continuous high oxygen saturation at the wound bed over a prolonged period of time indicates a nonhealing trend. Observe in Fig. 12(c) where four nonhealing cases (SC019, SC014, SC005, SC015) are shown, that the horizontal line of SO2 $= 0.6$ represents a reasonable threshold to estimate three of the four cases as nonhealing (i.e., SC015 is misclassified). Thus, we derived an empirical rule that if the wound bed SO2 > 0.6, the wound is nonhealing. To better characterize the multispectral SO2 assessment as a feature for healing trend analysis, we again perform logistic regression using the in-wound median SO2 as the sole feature. Fig. 12(d) shows the regression result. Observe how well the in-wound SO2 correlates with the healing status. We again note that our multispectral experimental results can become less reliable due to illumination variations induced during the data collection step.

C. Chemical Sensing Analysis Results

We have collected a total of 41 chemical sensing data sessions out of all 133 wound assessment sessions. The missing chemical sensing sessions were due to the missing or damaged RF sensing tags that occurred during handling and transportation.

As shown in Fig. 9(c), the RFID impedance response has real and imaginary components. While the real component has a single peak, the imaginary component has one peak and one

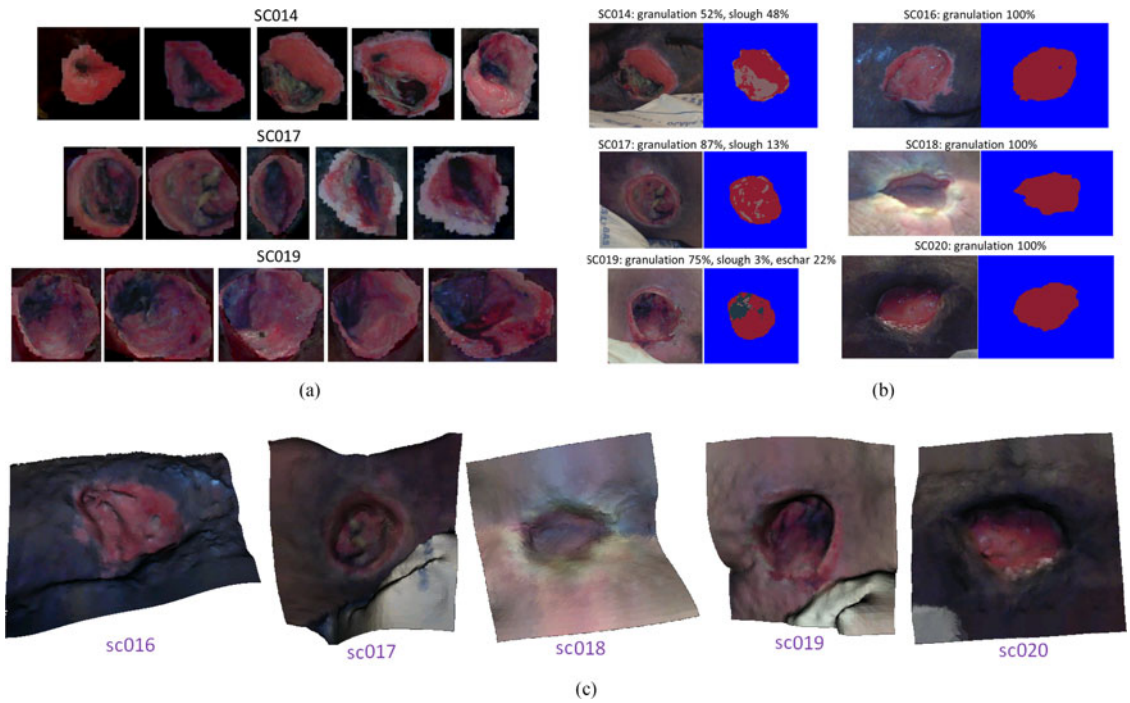

Fig. 11. (a–c) Wound measurements of length, width, depth, surface, and volume over time for subjects (a) SC014, (b) SC018, (c) SC019. (d-f) Scatter plots of the measured wound (d) length, (e) width, (f) depth versus manual measures in the unit of mm.

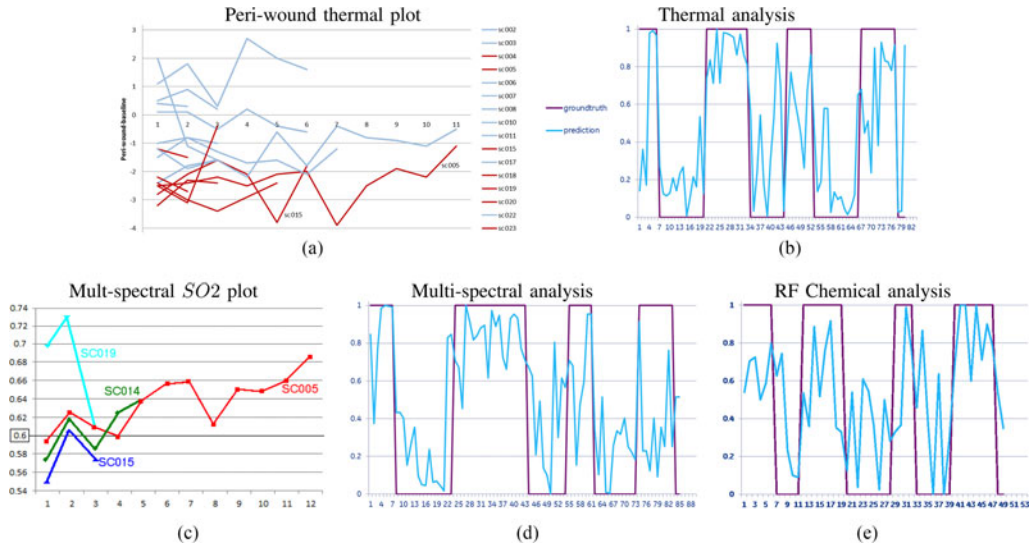

Fig. 12. Thermal, multispectral, and chemical analysis results. (a) Temperature difference plot between peri-wound T_p and normal skin (baseline) T_s for all patients over time, where the healing (blue) and nonhealing (red) cases obtained from the clinical notes are depicted. Observe the clear distinction between the two cases by the peri-wound feature f_p. (b) Healing trend prediction from logistic regression of the thermal features, where the *x*-axis depicts patient assessment sessions, and *y*-axis depicts the probabilities of healing (1) and nonhealing (0). Purple curves represent groundtruth and cyan curves represents individual prediction. (c) Multispectral oxygen saturation ($SO2$) plot of the wound bed for four nonhealing cases. (d) Healing trend prediction from multispectral logistic regression. (e) Healing trend prediction from RF chemical sensing repression.

trough. Thus, we have six parameters for each RFID response: 1) peak location of real component f_0, 2) response magnitude at f_0, 3) peak location of imaginary component f_1, 4) response magnitude at f_1, 5) trough location of imaginary component f_2, and 6) response magnitude at f_3. Note that as shown in Fig. 9(c), the RFID response is discrete at individual frequencies and the raw data may be noisy, thus we use the adjacent data near the peak and trough to fit the raw response and calculate the six parameters from the regression fit curve. Then, for each RF chemical sensing measurement, we calculate the difference between the sample and baseline for each of the above-mentioned parameters and thus the six RF sensing features as mentioned in Section III-J.

For building the logistic regression model, we have wound size measurement history for each patient. Thus, after calculating the six RF sensing feature parameters $x_i, i = 0, 1, ...5$, we use the wound size change as the indicator to label wound as healing ($y = -1$) and nonhealing ($y = 1$) for each RF sensing

sample. Then we use leave-one-out method to train the regression model and perform cross validation.

We trained a logistic regression model for the RF chemical analysis based on the six features described in Section III-J. We obtained coefficients 23.7404 and 1.0507 for *Real-Peak-Shift* and *Impedance,* respectively, 127.4927 and 0.3654 for *Imag-Peak-Shift* and *Impedance,* respectively, 43.3631 and 1.9828 for *Imag-Through-Shift* and *Impedance,* respectively. From this analysis, *Imag-Peak-Shift* is the most significant for healing trend prediction, as its regression coefficient is the highest. We obtained an error rate of 28.57% for the RF chemical analysis, which is slightly higher than the error rate of 23.75% from the thermal analysis. Fig. 12(e) shows the healing trend estimation from he RF chemical sensing.

V. Conclusion

We have presented a portable multimodal probe system as an aid to skin wound assessment and care. The system integrated five sensing modalities including EO, depth, thermal, multispectral imaging, and chemical sensing to provide real-time visual assessment of the wound. The developed analytic algorithms can not only perform wound size measurements by interactive wound segmentation and tissue classification followed by a 3-D reconstruction of the wound, but also it can perform thermal, spectral, and chemical vapor analysis of the wound for healing trend prediction. The system was developed and evaluated using a real-life patient dataset collected at a clinical site. Our wound volumetric measurement module and healing trend prediction modules provide a new means for objective healing progression assessment. To the best of our knowledge, our work is first of its kind in applying multispectral sensing and chemical odor analysis on live human subjects in a clinical setting. Our system is easily deployable for use in hospitals, clinics, and home environments. The integration of the GUI system to a web portal can assist patient data organization and support telehealth services.

Future work includes the collection of a larger dataset and the improvement of multispectral imaging acquisition to alleviate environmental variations. Specifically, tighter integration of chemical sensing with the multisensor analysis requires a sufficiently large dataset, such that GC-MS wound vapor concentrations and their correlations with respect to the healing process can be statistically quantified.

References

[1] D. Lahat, T. Adali, and C. Jutten, "Multimodal data fusion: An overview of methods, challenges, and prospects," *Proc. IEEE*, vol. 103, no. 9, pp. 1449–1477, Sep. 2015.

[2] P. K. Atrey, M. A. Hossain, A. E. Saddik, and M. S. Kankanhalli, "Multimodal fusion for multimedia analysis: A survey," *Multimedia Syst.*, vol. 16, no. 6, pp. 345–379, 2010.

[3] H. Medjahed, D. Istrate, J. Boudy, J.-L. Baldinger, and B. Dorizzi, "A pervasive multi-sensors data fusion for smart home healthcare monitoring," in *Proc. IEEE Fuzzy Syst.*, 2011, pp. 1466–1473.

[4] C. K. Sen *et al.*, "Human skin wounds: A major and snowballing threat to public health and the economy," *Wound Repair Regener.*, vol. 17, no. 6, pp. 763–771, 2009.

[5] D. Keast, C. Bowering, A. Evans, G. Mackeane, C. Burrows, and L. D'Souza, "Measure: A proposed assessment framework for developing best practice recommendations for wound assessment," *Wound Repair Regener.*, vol. 12, pp. S1–S17, 2004.

[6] H. Wannous, Y. Lucas, S. Treuillet, and B. Albouy, "A complete 3D wound assessment tool for accurate tissue classification and measurement," in *Proc. IEEE Int. Conf. Image Process.*, 2008, pp. 2928–2931.

[7] L. Wang, P. C. Pedersen, D. M. Strong, B. Tulu, E. Agu, and R. Ignotz, "Smartphone-based wound assessment system for patients with diabetes," *IEEE Bio. Engin.*, vol. 62, no. 2, pp. 477–488, Feb. 2015.

[8] M. Fauzi, I. Khansa, K. Catignani, G. Gordillo, C. Sen, and M. Gurcan, "Computerized segmentation and measurement of chronic wound images," *Comp. Bio. Med.*, vol. 60, pp. 74–85, 2015.

[9] Z. Cai, J. Han, L. Liu, and L. Shao, "RGB-D datasets using microsoft kinect or similar sensors: A survey," *Multimedia Tools Apps.*, vol. 76, pp. 4313–4355, 2016.

[10] K. Chong, A. Abdul-Ram, A. Hani, and F. Yap, "Volume assessment of various wound attributes models using 3d skin surface imaging," in *Proc. IEEE Int. Conf. Green Ubiquitous Technol.*, 2012, pp. 134–138.

[11] S. Barone, A. Paoli, and A. Razionale, "Assessment of chronic wounds by three-dimensional optical imaging based on integrating geometrical, chromatic and thermal data," *Proc. Inst. Mech. Eng.*, vol. 225, pp. 181–193, 2011.

[12] M. Romanelli, G. Gaggio, M. Coluccia, F. Rizzello, and A. Piaggesi, "Technological advances in wound bed measurements," *Wounds*, vol. 14, pp. 58–66, 2002.

[13] P. Unger, C. Fife, and D. Weir, "Capturing the essence of the wound evaluation," in *Proc. Today's Wound Clinic*, pp. 38–42, 2008.

[14] C. Ahn and R. Salcido, "Advances in wound photography and assessment methods," *Adv. Skin Wound Care*, vol. 21, no. 2, pp. 85–93, 2008.

[15] B. Shai and H. Maibach, "Wound healing, and ulcers of the skin," in *Diagnosis and Therapy—The Practical Approach*. Berlin, Germany: Springer, 2005.

[16] A. Hani, N. Eltegani, L. Arshad, S. Hussein, A. Jamil, and P. Gill, "Wound model reconstruction from three-dimensional skin surface imaging using the convex hull approximation method," *IET Image Process*, vol. 6, no. 5, pp. 521–533, Jul. 2011.

[17] D. Kosmopoulos and F. Tzevelekou, "Automated pressure ulcer lesion diagnosis for telemedicine systems," *IEEE Eng. Med. Biol. Mag.*, vol. 26, no. 5, pp. 18–22, Sep./Oct. 2007.

[18] J. Hardwicke, R. Thomson, A. Bamford, and N. Moiemen, "A pilot evaluation study of high resolution digital thermal imaging in the assessment of burn depth," *Burns*, vol. 39, pp. 76–81, 2013.

[19] G. Lu and B. Fei, "Medical hyperspectral imaging: A review," *J. Biomed. Opt.*, vol. 19, p. 010901, 2014.

[20] A. Chauhan, M. K. Goyal, and P. Chauhan, "GC-MS technique and its analyical applications in science and technology," *J. Anal. Bioanal. Technol.*, vol. 5, pp. 5–9, 2014.

[21] R. A. Potyrailo *et al.*, "Integration of passive multivariable RFID sensors into single-use biopharmaceutical manufacturing components," in *Proc. Int. Conf.IEEE RFID*, 2010, pp. 1–7.

[22] R. A. Potyrailo, C. Surman, N. Nagraj, and A. Burns, "Materials and transducers toward selective wireless gas sensing," *Chem. Rev.*, vol. 111, no. 11, pp. 7315–7354, 2011.

[23] M. Whitbeck and H. Guo, "Multiple landmark warping using thin-plate splines," in *Proc. IPCV*, 2006, pp. 256–263.

[24] C. Rother, V. Kolmogorov, and A. Blake, "Grabcut: Interactive foreground extraction using iterated graph cuts," *ACM Trans. Graph.*, vol. 23, no. 3, pp. 309–314, Aug. 2004.

[25] Y. Cheng, "Mean shift, mode seeking, and clustering," *IEEE Trans. Pattern Anal. Mach. Intell.*, vol. 17, no. 8, pp. 790–799, Aug. 1995.

[26] M.-C. Chang, F. F. Leymarie, and B. B. Kimia, "Surface reconstruction from point clouds by transforming the medial scaffold," in *Proc Sixth Int. Conf. 3-D Dig. Imag. Model.*, 2009, vol. 113, pp. 1130–1146.

[27] F. Bernardini, J. Mittleman, H. Rushmeier, C. Silva, and G. Taubin, "The ball-pivoting algorithm for surface reconstruction," *IEEE Trans. Vis. Comput. Graph.*, vol. 5, no. 4, pp. 349–359, Oct.–Dec. 1999.

[28] M. Kazhdan and H. Hoppe, "Screened poisson surface reconstruction," *ACM Trans. Graph.*, vol. 32, no. 3, pp. 29:1–29:13, Jul. 2013.

[29] M. Kazhdan, M. Bolitho, and H. Hoppe, "Poisson surface reconstruction," in *Proc. Symp. Geometry Process.*, 2006, pp. 61–70.

[30] C. B. Barber, D. P. Dobkin, and H. T. Huhdanpaa, "The Quickhull algorithm for convex hulls," *ACM Trans. Math. Softw.*, vol. 22, no. 4, pp. 469–483, Dec. 1996.

[31] C. K. Sen, "Wound healing essentials: Let there be oxygen," *Wound Repair Regenr.*, vol. 17, no. 1, pp. 1–18, 2009.

[32] F. Zou, C. Jin, R. R. Ross, and B. Soller, "Investigation of spectral interferences on the accuracy of broadband CW-NIRS tissue SO2 determination," in *Proc. Biomed. Opt. Express*, 2010, pp. 748–761.

[33] E. Stashenko and J. R. Martinez, "Gas chromatography-mass spectrometry," in *Advances in Gas Chromatography*, X. Guo, London, U.K.: Ed. Intech Open Science, 2014, ch. 1, pp. 1–38.
[34] R. A. Potyrailo, W. G. Morris, T. Sivavec, H. W. Tomlinson, S. Klensmeden, and K. Lindh, "RFID sensors based on ubiquitous passive 13.56-MHz RFID tags and complex impedance detection," *Wireless Commun. Mobile Comput.*, vol. 9, no. 10, pp. 1318–1330, 2008.

Ming-Ching Chang (M'08) received the Ph.D. degree from Brown University, Providence, RI, USA.

He is an Assistant Professor with the Department of Electrical and Computer Engineering, State University at Albany, Albany, NY, USA. He was a Lead Computer Scientist with GE Research. His research interest includes video analytics, computer vision, and artificial intelligence.

Ting Yu received the Ph.D. degree from Northwestern University, Evanston, IL, USA.

He is a Software Engineer with Google Cloud. He was a Senior Scientist with GE Research. His research interest includes computer vision, deep learning, real-time video analytics, and software systems.

Jiajia Luo received the Ph.D. degree from the University of Tennessee, Knoxville, TN, USA.

She is a research scientist with GE Research Albany, NY, USA. Her expertise includes video analytics, computer vision, and machine intelligence. Her research interest includes video analytics, computer vision, and machine intelligence.

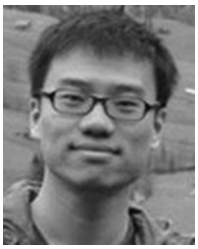

Kun Duan (M'14) received the Ph.D. degree from Indiana University, Bloomington, IN, USA.

He is a Research Engineering Lead with Snap Research. He was a computer scientist with the Global Research. His research interest includes object recognition, probabilistic graphical models, and deep learning.

Peter Tu is a Senior Principal Scientist for a group of 15 researchers in the field of multiview video analysis with the aim of acheiving reliable behavior recognition in complex environments at GE Research. He has more than 50 peer reviewed publications and has filed more than 25 U.S. patents.

Yang Zhao received the M.S. degree from the Beijing University of Aeronautics and Astronautics, Beijing, China, in 2006, and the Ph.D. degree from the University of Utah, Salt Lake City, UT, USA, in 2012.

He is a Research Engineer with GE Research. His research interests include signal processing, sensor networks, and real-time location systems.

Nandini Nagraj received the Ph.D. degree from the University of Illinois at Urbana-Champaign, Champaign, IL, USA.

She is the Team Leader of the Technical Operations with the Point of Care business, Siemens Healthineers, Erlangen, Germany. She was a Senior Scientist with GE Research. She has more than 15 peer-reviewed publications, 3 granted patents and 10 patent applications.

Vrinda Rajiv is a Principal Software Engineer with GE Research, Niskayuna, NY, USA. Her areas of expertise are software architecture, data analytics, decision sciences, process engineering, diagnostic, and prognostic technologies. She has more than 25 years of experience as a solution architect and a project lead.

Michael Priebe is a board certified physician in Physical Medicine and Rehabilitation, and Spinal Cord Injury Medicine. He is Chief of the Spinal Cord Injury Service with the Charlie Norwood VA Medical Center, Augusta, GA, USA. He provides primary and specialty care for inpatients and outpatient with spinal cord injury and disorders.

Elena A. Wood received the M.D. in 1994 and the Ph.D. degree in general oncology and medical informatics in 1998.

She is an Assistant Professor with the Department of Medicine, Medical College of Georgia, Augusta University, Augusta, GA, USA. Her research interests include designing and developing innovations and utilization of instructional technologies in medical education.

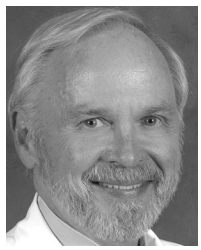

Maximillian Stachura was Director of the Center for Telehealth and Georgia Research Alliance Eminent Scholar in Telemedicine (1996-2017) with the Medical College of Georgia, Augusta University (MCG/AU). In 2017, he became Emeritus Professor of Medicine in telemedicine with MCG/AU, and continues his MCG/NeuroEndocrine practice and telemedicine consultant activities.